International Journal of Thermofluids 23 (2024) 100772

Contents lists available at ScienceDirect

International Journal of Thermofluids

journal homepage: www.sciencedirect.com/journal/international-journal-of-thermofluids

Inspection of numerical and fractional *CMC* and water-based hybrid nanofluid with power law and non-singular kernel: A fractal approach

Ahmed M. Abed [a,b], Hamna Shabbir [c], Niat Nigar [c], Ali Hasan Ali [d,e,f,g,*], Ali Raza [c,h]

[a] Department of the Industrial Engineering, College of Engineering, Prince Sattam Bin Abdulaziz University, Al Kharj 16273, Saudi Arabia
[b] Industrial Engineering Department, Zagazig University, Zagazig 44519, Egypt
[c] Department of Mathematics, Minhaj University Lahore, Pakistan
[d] Department of Mathematics, College of Education for Pure Sciences, University of Basrah, 61001 Basrah, Iraq
[e] Institute of the Mathematics, University of Debrecen, Pf. 400 H-4002 Debrecen, Hungary
[f] Department of Business Management, Al-imam University College, 34011 Balad, Iraq
[g] College of Engineering Technology, National University of Science and Technology, 64001 Dhi Qar, Iraq
[h] Department of Mathematics, University of Engineering and technology Lahore, Pakistan

ARTICLE INFO

Keywords:
Natural convection
Fractal fractional
Laplace transformation
Micro-channel
Nanofluids

ABSTRACT

A number of thermal devices might benefit from the usage of nanofluids in solar power. In this research, the idea of MHD mixed convective hybrid nanofluids including grapheme oxide (*GO*) and molybdenum disulfide (MoS_2) nanoparticles with water (H_2O) and Carboxymethyl Cellulose (*CMC*) as base fluids in a perpendicular channel to analyze the heat transfer of the flowing fluid with the help of recent definition of fractional derivatives namely Fractal fractional derivative. The problem is expressed as PDEs with beginning and boundary conditions, and it is analyzed analytically using the Laplace transform method. The velocity, temperature, and concentration measurements are also shown in series for their appropriate Laplace inverse. Delays in parameters like nanoparticle volume sharing rate have a significant influence on these techniques. Skin friction, Nusselt, and Sherwood numbers are computed for the longitudinal channel's left and right walls, and the necessary numerical results are presented in tabular format. As a result, it is discovered that the rate of heat transfer reduces as the volume percentage of nanoparticles and the Fractal time fractional value rise. Furthermore, when comparing nanofluids, water-based ($H_2O + GO + MoS_2$) hybrid nanofluids have a greater influence on governed model than ($CMC + GO + MoS_2$)-based hybrid nanofluids.

1. Introduction

The development of humanity has been strongly influenced by the notions of distinction and integration, which have been closely linked to the advancement of mathematics. Velocity and acceleration are the two most prominent applications of these two mathematical instruments. Further, we may utilize the idea of integration to describe the interface and dimension. There is little question that differential equations, integral equations, and modeling are among the most essential applications for these mathematical talents. The extant literature divides differential operators into two classes, each with its own set of subclasses. According to recent studies, compatible and fractals are among the most essential mathematical techniques for solving issues in local contexts, such as overcrowding and air quality. Specifically, these are issues that the conventional derivative cannot answer. The two recently developed differential operator studies have created new avenues for empirical and theoretical study, and these quantitative methodologies have attracted the curiosity of many young academics. These distinct differential operators might be used to simulate a wide range of natural physical issues. Newton's calculus can only be used to address problems with continuous space and bounds. Using the ordinary derivative operators in Newton's calculus, occurrences with porous frameworks and unsmooth boundaries may be described and analyzed. For example, the continuum fluid theory cannot explain how molecule size influences fluid turbulence in classical mechanics. Despite its relative freshness, little study has been conducted on this integral and differential operation. There is a link connecting fractal calculus and fractional calculus in [1], where Abdon Atangana demonstrates the fractal-fractional integral as well as differential operators and their connections to fractal calculus. In addition to providing various innovative concepts and numerical

* Corresponding author at: Institute of Mathematics, University of Debrecen, Pf. 400 H-4002 Debrecen, Hungary.
E-mail address: ali.hasan@science.unideb.hu (A.H. Ali).

https://doi.org/10.1016/j.ijft.2024.100772

Available online 23 July 2024

projections for the administrators, he also provided other suggestions that were relevant to real-world challenges. In [2], authors have investigated the entropy generation of a ternary hybrid nanofluid consisting of different nanoparticles flowing through a stretched sheet. Prince et al. [3] proposed an artificial intelligence (AI) based study for an MHD-based mixed convection hybrid nanofluid with magnetic field impact. They have also analyzed the entropy generation through AI tools. Tangirala et al. [4] studied the influence of heating conditions on the swirl flow consisting of a ternary hybrid nanofluid. Ahamed et al. [5] also instigated the thermal performance of a hybrid nanofluid flowing through a double-dimpled tube. They constructed numerical simulations and used computational algorithms to solve the mathematical model equations.

To enhance the thermodynamic qualities of base fluids, nanofluids are mixtures of nanoscale particles that are frequently deferred in the base fluid. Focus has turned to the use of various base fluids, like water and ethylene together with different nanoparticles, so as to boost surface area and heat expansion of common liquids. The fact that common fluids have poor thermal conductivities and can be made more thermally conductive by mixing 1 % of dispersed nanoparticles from 40 to 150 % cannot be avoided. This unique product was created by mixing at least two materials with numerous corporeal and chemical qualities, like thermal conductivity and heat flow. Traditional base fluids often have adequate heat transmission rate, thermal conduction, and heating ability for mechanical use. To enhance these qualities, Maxwell [6] was the first person to suggest dispersing micro-sized particles in ordinary base fluids. As a result, there was a requirement to reduce the dimensions of particles, and to address the matter, Choi and Eastman [7] established the concept of nano-sized particle dissemination in base fluids in 1995. Later on, this became a hot issue among scholars, and several papers on the uses of nanofluids in the fields of science and technology were published. Devendiran et al. [8] examined the preparation and different applications of nanofluids with different characterized nanoparticles. Later on, Mahboobtosi et al. [9] investigated the performance and enhancement of ternary-type hybrid nanofluid flowing through a stretched cylinder. Aman et al. [10] used the Caputo-time fractional definition to study the heat transfer of water-based hybrid nanofluid. Furthermore, they have also discussed and explained the physical applications of solar energy systems. Khan et al. [11] studied the hybrid optimization for the biosynthesized nanofluid to enhance the thermal performance of solar thermal collectors. Raza et al. [12] analyzed the fractional Jeffery-type hybrid nanofluid flowing through a poured channel utilizing two definitions of fractional definitions, namely Prabhakar and fractal fractional derivatives. Adding only one nanoparticle produces pleasant outcomes, but changes may disrupt some of the features of the base fluids, such as the dimension, lubricity, division voltage, and the dielectric property of traditional fluids [13]. Hybrid nanofluids, which float numerous kinds of nanoparticles in a base fluid, have been employed in various science and engineering disciplines to enhance their properties and productivity [14]. Domairry et al. [15] pragmatic a free-convective non-Newtonian copper-water nanofluid between two indefinitely parallel vertical flat surfaces. Prandtl, Grashof, Schmidt, and Brinkman numbers for fluids, as well as the chemical reaction parameter, will catch our attention after the precise solutions have been determined, and their effects on the modeling will be provided and explained from a physical standpoint. Farooq et al. [16] used a modified Bessel equation and the Laplace transformation, the shear stress and speed field associated with the vibratory gesture of a fractional Burgers' fluid model in an endlessly circular cylinder are investigated. Asjad et al. [17] premeditated the unstable and incompressible viscid fluid flow with CPC-type fractional derivative. Porosity and MHD are also taken into account as additional consequences.

Furthermore, it is noted that all current fractional operators with power law Caputo (C), exponential law Caputo-Fabrizio (CF), and Mittage-Leffler law Atangana-Baleanu (AB) are less suitable for illustrating the decrease of fluid velocity than the constant proportional Caputo type operator. Yue et al. [18] looked for the KS equation, and novel explicit wave solutions were created. The Khater approach was utilized to obtain novel wave solutions in various forms which was used in the phenomenon of pressure waves passing through the mixing of liquid-gas bubbles under thermodynamic conditions. Sun et al. [19] concluded the dynamics of spatially nonlocal velocity, which was the force behind non-Newtonian fluid flow, predicted by promising *FD* models. Arafa et al. [20] demonstrated the time-fractional derivative is used to evaluate an unstable convection-radiation interaction flow of power-law non-Newtonian nanofluids. Tayebi et al. [21] investigated the natural cooling in the nanofluid hybrid system using a magnetic field and a square container. Manjunatha et al. [22] examined the flow of $Cu - Al_2O_3 - H_2O$ hybrid nanofluids with varying viscosities. Lee et al. [23] demonstrated that the inclusion of nanoparticles increased the thermal and mechanical features of the base fluid. In furtherance of highlighting the advantages of utilizing hybrid nanofluids above pure water in hydraulic blocks, Bahiraei et al. [24] observed that employing the nanofluid increased the effectiveness of the heat sink. Mendoza et al. [25] analysed the TiO_2 and $TiO_2 - SiO_2$ nanoparticles based solid and compare the results with their photo-catalytic possessions.

The differential modeling technique was used to convert the leading model into an ODE. They observed that the thermal boundary increased as the volume fraction of nanoparticles increased. Layer become thinner as the velocity boundary layer got thicker. Thermal conductivity is just one of the numerous benefits that nanofluids can provide. Xu et al. [26] proposed the advanced heat and mass transfer kinetics of hybrid nanofluid flow through closed- continuous channel. Casson nanofluid parallel diffusion flux patterns across an everlasting vertical screen were shown by kumar et al. [27]. Yilmaz et al. [28] conducted an experimental study comparing the non-Newtonian and Newtonian runs through porous material. The application of freshly designed fractal fractional multipliers employing power-law bases in water dynamics is presented by Agarwal et al. [29]. MHD viscoelastic liquid circulates through two plates, with the top plate advancing constantly and the smaller plate remaining stationary. A fractal fractional derivative function featuring a power law kernel can be utilized to construct the governing equation. Abbas et al. [30] found that non-Newtonian flow of liquids is crucial in production and industrial procedures. The current research's major purpose is to build and enhance a Newtonian flow model in a channel with two adjacent vertical plates. Unlike previous fractional derivatives, the Prabhakar generator employed the three components of the ML translation as its kernel, rendering it more general and complex. Gangadhar et al. [31] studied second-grade MHD fluid's intermittent and insoluble flow on a vertical vibrating plate with thermal radiation and applied magnetic field. The most advanced and practical fractional interpretation is the Prabhakar fractional derivative, which often relies on modified Fourier's and Fick's laws in addition to non-dimensional managed models into fractional models. Shah et al. [32] examined a Casson-type fluid through computational intelligence for dynamic nanofluid model that is unstable and incompressible and is traveling on an inclined surface. Almutairi et al. [33] studied the applications of time Fractal Fractional derivative with power-law kernel for Newton's interpolation polynomials. Abro & Atangana [34] presented a fractal-fractional usual of convective fluid gesture in a revolving hollow with inhomogeneous external heating. Arif et al. [35] looked a novel kind of fractional derivative with a power Law kernel called fractal-fractional derivative has various uses in practical issues. Akgul et al. [36] utilized the Fractal-fractional definition to simulate the chemical degradation in the bioreactor. Ali et al. [37] studied the fractal-fractional non-linear viscoelastic fluid using the finite difference method's numerical scheme.

To the best of the author's knowledge, still, no research has been done using the recent definition of fractional derivatives, namely as Fractal fractional derivatives, to investigate the unstable and incompressible Hybrid nanofluid (consisting *CMC*, H_2O as base fluid, and

MoS_2,GO as nanoparticles) flow of elemental fluxes under the impact of magnetic field and inclination. In this study, we have assumed two hybrid nanofluids ($CMC + MoS_2 + GO$), ($H_2O + MoS_2 + GO$) are flowing in an oscillating channel with a porosity surface. We utilized the Fractal non-integer order derivative, the most recent and revised definition of fractional derivatives. We also employed the integral transform, namely the Laplace transformation, to solve the governed non-dimensional PDE. Finally, the graphical and tabular comparison and impact of all limitations are examined. The overlapping of curves in the comparative study with previous literature validates this study's outcomes.

Nomenclature:

Symbol		Quantity	Unit
w_1	:	Fluid velocity	(m/s)
t	:	Times	(s)
g	:	Gravity acceleration	(m/s^2)
k_{nf}	:	Thermal conductivity of the nanofluid	(W/mk)
C_f	:	Skin friction	$(-)$
ρ_{nf}	:	Nanofluid density	(Kg/m^3)
U_0	:	Characteristic velocity	(ms^{-1})
θ	:	The angle of magnetic inclination	$(-)$
Gm	:	Mass Grashof number	$(-)$
μ_{nf}	:	Dynamic viscosity	(Kg/ms)
Pe	:	Peclet number	$(-)$
T_w	:	Wall temperature	(K)
Gr	:	Heat Grashof number	$(-)$
T_d	:	Ambient temperature	(K)
α, β	:	Fractional parameters	$(-)$
Sc	:	Schmidt number	$(-)$
M	:	Magnetic field	$(-)$
s	:	Laplace transform variable	$(-)$
B_o	:	Magnetic field strength	(Kg/s^2)
C_p	:	Specific heat at constant pressure	(J/kgK)
β_T	:	Thermal expansion coefficient	$(1/k)$
σ	:	Electrical conductivity	$(-)$
Nu	:	Nusselt number	$(-)$
Sh	:	Sherwood number	$(-)$

2. Problem description

Here we have presumed that an incompressible Newtonian fluid in two infinite plates (micro-channel) which are parallel and place horizontally. Distance between plates is$d$. It is presumed that both plates are in rest position and temperature is constant at initially. With time $t > 0$, due to the oscillation of one plate and due to the variation in temperature field, the hybrid nanofluids starts to flow with a constant velocity U_0. Flow of the fluid is also due to free convection, as illustrated in Fig 1.

- The microchannel has an unlimited length and a width of h.
- The microchannel oscillates perpendicular to the y-axis and along the x-axis.
- The system's temperature isT_0at time$t = 0$.
- The temperature rises from$T_0$to$T_w$after$t > 0$.
- Fluid moves more quickly in the x direction due to variations in temperature field and pressure gradient.
- An inclined magnetic field (θ) with aB_0intensity operates against the flow direction.
- The CMC and water based hybrid nanofluids are considered with different nanoparticles.

Governing equations for the flowing hybrid nanofluid in microchannel will be as follows [10]

$$\rho_{nf}\frac{\partial V_1(\xi,t)}{\partial t} = \mu_{nf}\frac{\partial^2 V_1(\xi,t)}{\partial \xi^2} + g(\rho\beta_T)_{nf}(\vartheta_1(\xi,t) - \vartheta_o) - \sigma_{nf}B_o^2 sin(\theta)V_1(\xi,t) + g(\rho\beta_c)_{nf}(\psi_1(\xi,t) - \psi_o) \tag{1}$$

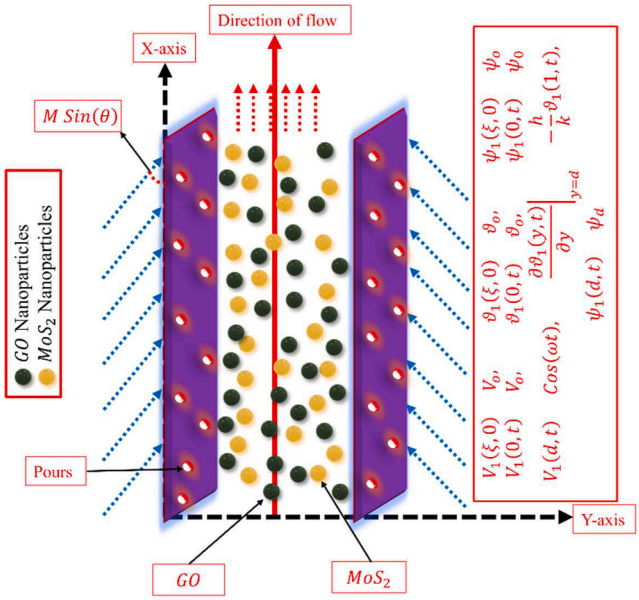

Fig. 1. Geometry of flow of different nanoparticles based hybrid nanofluids.

$$(\rho C_p)_{nf}\frac{\partial \vartheta_1(\xi,t)}{\partial t} = \frac{k_{nf}}{k_f}\frac{\partial^2 \vartheta_1(\xi,t)}{\partial \xi^2} + 4\alpha_o^2(\vartheta - \vartheta_o) \tag{2}$$

$$\frac{\partial \psi_1(\xi,t)}{\partial t} = D_{nf}\frac{\partial^2 \psi_1(\xi,t)}{\partial \xi^2} \tag{3}$$

with the boundary conditions:

$$V_1(\xi,0) = V_o,\ \vartheta_1(\xi,0) = \vartheta_o,\ \psi_1(\xi,0) = \psi_o \tag{4}$$

$$V_1(0,t) = V_o,\ \vartheta_1(0,t) = \vartheta_o,\ \psi_1(0,t) = \psi_0 \tag{5}$$

$$V_1(d,t) = Cos(\omega t),\ \left.\frac{\partial \vartheta_1(y,t)}{\partial y}\right|_{y=d} = -\frac{h}{k}\vartheta_1(1,t),\ \psi_1(d,t) = \psi_d \tag{6}$$

To non-dimensionalize the above mathematical model with its perspective governed equations and conditions utilizing the following constraints

$$\overline{y} = \frac{\xi}{l}, \overline{w_1} = \frac{V_1}{U_o},\ \overline{t} = \frac{U_o t}{l}, \overline{d} = \frac{d}{l}, M = \frac{\sigma_f B_o^2 d^2}{\mu},\ Re = \frac{U_o d}{\nu}, Gr = \frac{g\beta_T d^2(\vartheta_d - \vartheta_o)}{\nu U_o},\ Gm = \frac{g\beta_C d^2(\psi_d - \psi_o)}{\nu U_o}, Pe = \frac{\mu C_p Re}{k} \tag{7}$$

After working on the non-denationalization, the simplified equations will be:

$$\phi_1 \mathrm{Re}\frac{\partial w_1\ (y,t)}{\partial t} = \phi_2\frac{\partial^2 w_1(y,t)}{\partial y^2} - \left(Msin(\theta) + K_{eff}\right)w_1(y,t) + \phi_3 Gr T_1(y,t) + \phi_4 Gm C_1(y,t) \tag{8}$$

$$\mathrm{Pe}\frac{\partial T_1\ (y,t)}{\partial t} = \frac{\partial^2 T_1(y,t)}{\partial y^2} \tag{9}$$

$$\Pi_1\frac{\partial C_1\ (y,t)}{\partial t} = \frac{\partial^2 C_1(y,t)}{\partial y^2} \tag{10}$$

where ϕ_1,ϕ_2,ϕ_3,Π_1 are constants calculated during mathematical work. w_1,T_1,C_1 are the non-dimensional velocity, temperature, and concentration, respectively. Furthermore, M is representing the magnetic field, θ is an inclination of the magnetic field, Gr is the heat Grashof number,

Gm mass Grashof number, *Re* is the Reynold number, and *Pe* is Peclet number.

The Dimensionless boundary conditions are:

$$= \begin{cases} w_1(y,0)=0,\ T_1(y,0)=0,\ C_1(y,0)=0, t=0 \\ w_1(0,t)=0,\ T_1(0,t)=0,\ C_1(0,t)=0, t>0 \\ w_1(d,t)=cos(\omega t),\ \left.\dfrac{\partial T_1}{\partial y}\right|_{y=d} = -(1+T(d,t)),\ C_1(d,t)=1, y=d \end{cases} \tag{11}$$

Table 1 shows the thermo-physical properties of basic quantities, and Table 2 shows the Considered nanofluids with their thermal characteristics [38].

Fractal Integral: A power law for the function a continuous function y(x) in terms of RL-form may be defined as

$${}^{FFP}\mathfrak{D}_x^{\alpha,\beta} y(x) = \frac{1}{\Gamma(1-\alpha)} \frac{d}{dx^\beta} \int_0^x y(t)(x-t)^{-\alpha} dt, 0<\alpha,\beta\le 1,$$

$$\frac{dy(t)}{dx^\beta} = \lim_{x\to t} \frac{y(x)-y(t)}{x^\beta - t^\beta},$$

Laplace Transformation: Consider $y(x)$ for instance where$(x>0)$. The Laplace integral offers a well-defined continuous function called the LT of $y(x)$ as $Y(s)$ or $\mathscr{L}\{y(x)\}$

$$\mathscr{L}\{y(x)\} = Y(x) = \int_0^\infty exp(-sx) f(x) dx,$$

Fractal Laplace Transformation: The fractal-Laplace of a continuous function $g(x)$ can be defined as [39]

$${}^{F}\mathscr{L}_p^\alpha\{g(x)\} = G(x) = \int_0^\infty exp(-sx) x^{\alpha-1} g(x) dx,$$

3. Fractional model

In this section, the Fractal fractional exemplary is represented. As all the governed equations of our non-dimensional model (7)-(9) are time dependent. So by employing the Fractal integral and derivative operator, we get the fractional model as follows.

Table 2
Considered nanofluids with their thermal characteristics.

Material	*CMC*	H_2O	MOS_2	*GO*
$\rho(kg/m^3)$	997	997.1	5060	1800
$C_p(J/kgK)$	4179	4179	397.20	717
$k(W/mK)$	0.613	0.613	904.4	5000
$\beta_T(K^{-1})$	20×10^{-5}	21×10^{-5}	2.842×10^{-5}	2.84×10^{-4}

$$\phi_1 \mathrm{Re}\left[{}^{FFP}\mathfrak{D}_t^{\alpha,\beta} w_1(y,t)\right] = \beta t^{\beta-1}\left[\phi_2 \frac{\partial^2 w_1(y,t)}{\partial y^2} - \left(M\sin(\theta)+K_{eff}\right) w_1(y,t) + \phi_3 Gr T_1(y,t) + \phi_4 Gm C_1(y,t)\right] - \frac{w_1(y,0)}{\Gamma(1-\alpha)} t^{-\alpha} \tag{12}$$

$$Pe\left[{}^{FFP}\mathfrak{D}_t^{\alpha,\beta} T_1(y,t)\right] = \beta t^{\beta-1}\left\{\frac{\partial^2 T_1(y,t)}{\partial y^2}\right\} - \frac{T_1(y,0)}{\Gamma(1-\alpha)} t^{-\alpha} \tag{13}$$

$$\Pi_1\left[{}^{FFP}\mathfrak{D}_t^{\alpha,\beta} C_1(y,t)\right] = \beta t^{\beta-1}\left\{\frac{\partial^2 C_1(y,t)}{\partial y^2}\right\} - \frac{C_1(y,0)}{\Gamma(1-\alpha)} t^{-\alpha} \tag{14}$$

Where ${}^{FFP}\mathfrak{D}_t^{\alpha,\beta}$ signifying the Fractal fractional operator.

4. Solution of fractional model

The explanation of governed fractional model will be resolved by retaining the LT on the fractional Eq. (12)-(16).

4.1. Analysis of temperature field

To analyze the clarification of thermal profile by engaging the LT on the administrated fractional Eq. (11)

$$\mathrm{Pe}[s^\alpha \overline{T_1}(y,s) - \overline{T_1}(y,0)] = \beta\,\Gamma(\beta) s^{-\beta}\left\{\frac{\partial^2 \overline{T_1}(y,s)}{\partial y^2}\right\} - \frac{\overline{T}_1(y,0)}{\Gamma(1-\alpha)} q^{1-\alpha} \tag{15}$$

With corresponding transformed conditions

$$\overline{T_1}(0,s) = 0,\ \left.\frac{\partial \overline{T}}{\partial y}\right|_{y=d} = -\left(\frac{1}{s} + \overline{T}(d,s)\right),$$

By utilizing the above conditions, solving and simplifying the Eq. (13), we get the thermal profile as follows

Table 1
The thermo physical properties of basic quantities.

Thermal features	Hybrid Nanofluid
Density	$\rho_f = \dfrac{\rho_{hnf}}{\left((1-\varphi_2)\left((1-\varphi_1)+\varphi_1\frac{\rho_{s1}}{\rho_f}\right)+\varphi_2\rho_{s2}\right)}$
Dynamic Viscosity	$\mu_f = \mu_{hnf}(1-\varphi_1)^{2.5}(1-\varphi_2)^{2.5}$
Electrical conductivity	$\sigma_{bf} = \dfrac{\sigma_{hnf}}{\left(1+\frac{3\varphi(\varphi_1\sigma_1+\varphi_2\sigma_2-\sigma_{bf}(\varphi_1+\varphi_2))}{(\varphi_1\sigma_1+\varphi_2\sigma_2+2\varphi\sigma_{bf}-\varphi\sigma_{bf}(\varphi_1\sigma_1+\varphi_2\sigma_2-\sigma_{bf}(\varphi_1+\varphi_2)))}\right)}$
Thermal conductivity	$k_{bf} = \dfrac{k_{hnf}}{\left(\frac{k_{s2}+(n-1)k_{bf}-(n-1)(k_{bf}-k_{s2})\varphi_2}{k_{s2}+(n-1)k_{bf}+(k_{bf}-k_{s2})\varphi_2}\right)}$ and $k_f = \dfrac{k_{bf}}{\left(\frac{k_{s1}+(n-1)k_f-(n-1)(k_f-k_{s1})\varphi_1}{k_{s1}+(n-1)k_f+(k_f-k_{s1})\varphi_1}\right)}$
Heat capacitance	$(\rho C_p)_s = \dfrac{(\rho C_p)_{hnf}}{(1-\varphi_2)\left((1-\varphi_1)+\varphi_1\frac{(\rho C_p)_{s1}}{(\rho C_p)_f}\right)+\varphi_2(\rho C_p)_{s2}}$
Thermal Expansion Coefficient	$(\rho\beta)_f = \dfrac{(\rho\beta)_{hnf}}{(1-\varphi_2)\left((1-\varphi_1)+\varphi_1\frac{(\rho\beta)_{s1}}{(\rho\beta)_{f1}}\right)+\varphi_2(\rho\beta)_{s2}}$

$$\overline{T}_1(y,s) = \frac{1}{\sqrt{\frac{Pe\ s^{\alpha+\beta}}{\beta\Gamma(\beta)}}-1}\ \frac{e^{y\sqrt{\frac{Pe\ s^{\alpha+\beta}}{\beta\Gamma(\beta)}}} - e^{-y\sqrt{\frac{Pe\ s^{\alpha+\beta}}{\beta\Gamma(\beta)}}}}{e^{\sqrt{\frac{Pe\ s^{\alpha+\beta}}{\beta\Gamma(\beta)}}} - e^{-\sqrt{\frac{Pe\ s^{\alpha+\beta}}{\beta\Gamma(\beta)}}}}$$
$$= \frac{1}{\sqrt{\frac{Pe\ s^{\alpha+\beta}}{\beta\Gamma(\beta)}}-1}\ \frac{Sinh\left(y\sqrt{\frac{Pe\ s^{\alpha+\beta}}{\beta\Gamma(\beta)}}\right)}{Sinh\left(\sqrt{\frac{Pe\ s^{\alpha+\beta}}{\beta\Gamma(\beta)}}\right)} \tag{16}$$

The above solution can be inscribed in more abridged form as

$$\overline{T}_1(y,s) = \frac{1}{\sqrt{\frac{Pe\,s^{\alpha+\beta}}{\beta\Gamma(\beta)}}-1}\sum_{\alpha_1=0}^{\infty}\left(e^{-(2\alpha_1+1-y)\sqrt{\left(\frac{Pe\,s^{\alpha+\beta}}{\beta\Gamma(\beta)}\right)}} + e^{-(2\alpha_1+1+y)\sqrt{\left(\frac{Pe\,s^{\alpha+\beta}}{\beta\Gamma(\beta)}\right)}}\right) \tag{17}$$

Now the relevant series form of exponential function can be expressed as

$$\overline{T}_1(y,s) = \sum_{\alpha=0}^{\infty}1 + \frac{(\mathrm{Pe})^{\frac{\alpha}{2}}\Gamma\left(\frac{\alpha}{2}+1\right)}{\alpha!\Gamma(\beta)}s^{-\frac{n(\alpha+\beta)}{2}} + \left[\sum_{\alpha_1=0}^{\infty}\sum_{\alpha_2=1}^{\infty}\right.$$
$$\left.\times\sum_{\alpha_3=0}^{\infty}\frac{(y-2\alpha_1-1)^{\alpha_2}(Pe)^{\frac{\alpha_3}{2}}\Gamma\left(\frac{\alpha+\beta}{2}+\alpha_3\right)}{\alpha_1!\alpha_3!\Gamma\left(\frac{Pe\beta c_3}{2}\right)}\frac{1}{s^{Pe\alpha_3-\frac{\alpha_2}{2}+\frac{\alpha_2\beta}{2}+Pe\,\beta+1}}\right]$$
$$-\left[\sum_{c_1=0}^{\infty}\sum_{c_2=1}^{\infty}\right.$$
$$\left.\times\sum_{c_3=0}^{\infty}\frac{(-y-2c_1-1)^{c_3}(Pe)^{\frac{c_3}{2}}\Gamma\left(\frac{\alpha+\beta}{2}+c_1\right)}{c_3!c_1!\Gamma\left(\frac{Pe\beta c_3}{2}\right)}\frac{1}{s^{Pec_3-\frac{c_2}{2}+\frac{c_2\beta}{2}+Pe\,\beta+1}}\right],$$

By taking the Laplace inverse

$$T_1(y,t) = \sum_{n=0}^{\infty}\delta(1) + \frac{(\mathrm{Pe})^{\frac{n}{2}}\Gamma\left(\frac{n}{2}+1\right)}{n!\Gamma(\beta)\Gamma\left(\frac{n\alpha}{2}+\frac{n\beta}{2}\right)}\frac{1}{t^{1-\frac{n(\alpha+\beta)}{2}}} +$$
$$\left[\sum_{a_1=0}^{\infty}\sum_{a_2=1}^{\infty}\sum_{a_3=0}^{\infty}\frac{(y-2a_1-1)^{a_2}(Pe)^{\frac{a_3}{2}}\Gamma\left(\frac{\alpha+\beta}{2}+a_3\right)}{a_1!a_3!\Gamma\left(\frac{Pe\beta c_3}{2}\right)\Gamma\left(1-\frac{a_2}{2}+Pea_1+\frac{a_2\beta}{2}+Pe\,\beta\right)}t^{-\frac{a_2}{2}+Pe\,a_3+\frac{a_2\beta}{2}+Pe\,\beta}\right] -$$
$$\left[\sum_{c_1=0}^{\infty}\sum_{c_2=1}^{\infty}\sum_{c_3=0}^{\infty}\frac{(-y-2c_1-1)^{c_3}(Pe)^{\frac{c_3}{2}}\Gamma\left(\frac{\alpha+\beta}{2}+c_1\right)}{c_3!c_1!\Gamma\left(\frac{Pe\beta c_3}{2}\right)\Gamma\left(1-\frac{c_2}{2}+Pec_1+\frac{c_2\beta}{2}+Pe\,\beta\right)}t^{Pe\,\beta-\frac{c_2}{2}+Pe\,c_3+\frac{c_2\beta}{2}}\right] \tag{18}$$

Which is the mandatory solution of heat profile.

4.2. Analysis of concentration field

Again, like thermal profile, to examine the concentration profile by retaining the LT on fractional model Eq. (12)

$$\Pi_1[s^{\alpha}\overline{C_1}(y,s) - C_1(y,0) = \beta\,\Gamma(\beta)s^{-\beta}\left\{\frac{\partial^2\overline{C_1}(y,s)}{\partial y^2}\right\} - \frac{\overline{C_1}(y,0)}{\Gamma(1-\alpha)}s^{1-\alpha},$$

With transformed conditions

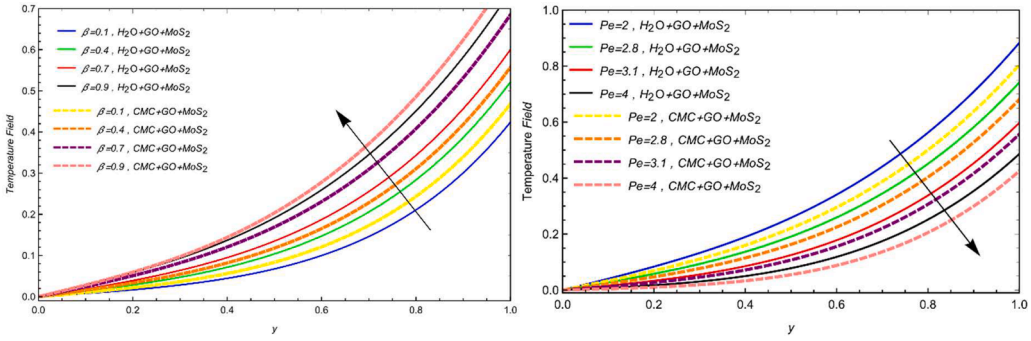

Fig. 2. Impact of fractional constraint β and Peclet number *Pe* on temperature field with α = 0.4, *t* = 0.8, φ = 0.02.

$$\overline{C}_1(0,s)=0,\ \overline{C}_1(d,s)=\frac{1}{s},$$

Using above conditions, the concentration profile will be as follows

$$\overline{C}_1(y,q)=\frac{1}{s}\frac{e^{y\sqrt{\frac{\Pi_1\ s^{\alpha+\beta}}{\beta\Gamma(\beta)}}}-e^{-y\sqrt{\frac{\Pi_1\ s^{\alpha+\beta}}{\beta\Gamma(\beta)}}}}{e^{\sqrt{\frac{\Pi_1\ s^{\alpha+\beta}}{\beta\Gamma(\beta)}}}-e^{-\sqrt{\frac{\Pi_1\ s^{\alpha+\beta}}{\beta\Gamma(\beta)}}}}=\frac{1}{s}\frac{sinh\left(y\sqrt{\frac{\Pi_1\ s^{\alpha+\beta}}{\beta\ \Gamma(\beta)}}\right)}{sinh\left(\sqrt{\Pi_1\ \frac{s^{\alpha+\beta}}{\beta\ \Gamma(\beta)}}\right)} \tag{19}$$

Above exponential form can be written as simplified form as

$$\overline{C}_1(y,q)=\frac{1}{s}\sum_{\alpha_1=0}^{\infty}\left(e^{-(2\alpha_1+1-y)\left(\frac{\Pi_1\ s^{\alpha+\beta}}{\beta\ \Gamma(\beta)}\right)^{\frac{1}{2}}}+e^{-(2\alpha_1+1+y)\left(\frac{\Pi_1\ s^{\alpha+\beta}}{\beta\ \Gamma(\beta)}\right)^{\frac{1}{2}}}\right),$$

Now the relevant series form of exponential function can be expressed as

$$\overline{C}_1(y,q)=\frac{1}{s}+\left[\sum_{\alpha_1=0}^{\infty}\sum_{\alpha_2=1}^{\infty}\sum_{\alpha_3=0}^{\infty}\frac{(y-2\alpha_1-1)^{\alpha_2}(\Pi_1)^{\frac{\alpha_3}{2}}\Gamma\left(\frac{\alpha+\beta}{2}+\alpha_3\right)}{\alpha_1!\alpha_3!\Gamma\left(\frac{\beta\alpha_3}{2}\right)}\frac{1}{s^{\alpha\alpha_3-\frac{\alpha_2}{2}+\frac{\alpha_2\beta}{2}+1}}\right]-\left[\sum_{c_1=0}^{\infty}\sum_{c_2=1}^{\infty}\sum_{c_3=0}^{\infty}\frac{(-y-2c_1-1)^{c_3}(\Pi_1)^{\frac{c_3}{2}}\Gamma\left(\frac{\alpha+\beta}{2}+c_1\right)}{c_3!c_1!\Gamma\left(\frac{\beta c_3}{2}\right)}\frac{1}{s^{\alpha c_1+\frac{c_3\beta}{2}-\frac{c_3}{2}+1}}\right],$$

By taking the Laplace inverse

$$C_1(y,t)=1+\left[\sum_{a_1=0}^{\infty}\sum_{a_2=1}^{\infty}\sum_{a_3=0}^{\infty}\frac{(y-2a_1-1)^{a_2}(\Pi_1)^{\frac{a_3}{2}}\Gamma\left(\frac{\alpha+\beta}{2}+a_3\right)}{a_1!a_3!\Gamma\left(\frac{\beta a_3}{2}\right)\Gamma\left(1-\frac{a_2}{2}+\alpha a_1+\frac{a_2\beta}{2}\right)}t^{-\frac{a_2}{2}+\alpha a_1+\frac{a_2\beta}{2}}\right]-\left[\sum_{c_1=0}^{\infty}\sum_{c_2=1}^{\infty}\sum_{c_3=0}^{\infty}\frac{(-y-2c_1-1)^{c_3}(\Pi_1)^{\frac{c_3}{2}}\Gamma\left(\frac{\alpha+\beta}{2}+c_1\right)}{c_3!c_1!\Gamma\left(\frac{\beta c_3}{2}\right)\Gamma\left(1-\frac{c_2}{2}+\alpha c_1+\frac{c_2\beta}{2}\right)}t^{-\frac{c_3}{2}+\alpha c_2+\frac{c_2\beta}{2}}\right] \tag{20}$$

which is the required solution of absorption profile.

4.3. Analysis of velocity field

For the velocity field, employing the LT on the governed fractional Eq. (12)

$$\phi_1 Re[s^{\alpha}\overline{w}_1(y,s)-w_1(y,0)]=\ \beta\ \Gamma(\beta)s^{-\ \beta}\left[\phi_2\frac{\partial^2\overline{w}_1(y,s)}{\partial y^2}-(M\sin(\theta)+K_{eff})\overline{w}_1(y,s)+\phi_3 Gr\overline{T}_1(y,s)+\phi_4 Gm\overline{C}_1(y,s)\right]-\ \frac{\overline{C}_1(y,0)}{\Gamma(1-\alpha)}s^{1-\alpha} \tag{21}$$

Also employing the LT on boundary conditions

$$\overline{w}_1(0,s)=0,\ \overline{w}_1(d,s)=\frac{s}{s^2+\omega^2},$$

Using the above conditions with thermal and concentration fields, we get the solutions of velocity profile as follows

$$\overline{w}_1(y,s)=\left(\frac{s}{s^2+\omega^2}+\frac{\Omega_7\ Gr}{s\left(\sqrt{\Omega_9\ s^{\alpha+\beta}}-1\right)}\ \frac{1}{\Omega_9\ s^{\alpha+\beta}-(\Omega_4 q^{\alpha+\beta}+\Omega_6)}+\frac{\Omega_8\ Gm}{s}\frac{1}{\Omega_{10}\ s^{\alpha+\beta}-(\Omega_4 q^{\alpha+\beta}+\Omega_6)}\right)\frac{sinh\left(y\sqrt{\Omega_4 q^{\alpha+\beta}+\Omega_6}\right)}{sinh\left(\sqrt{\Omega_4 q^{\alpha+\beta}+\Omega_6}\right)}-\frac{1}{\Omega_9\ s^{\alpha+\beta}-(\Omega_4 q^{\alpha+\beta}+\Omega_6)}\frac{\Omega_7\ Gr}{s\left(\sqrt{\Omega_9\ s^{\alpha+\beta}}-1\right)}\frac{sinh\left(y\sqrt{\Omega_9\ s^{\alpha+\beta}}\right)}{sinh\left(\sqrt{\Omega_9\ s^{\alpha+\beta}}\right)}-\frac{\Omega_8\ Gm}{s}\frac{1}{\Omega_{10}\ s^{\alpha+\beta}-(\Omega_4 q^{\alpha+\beta}+\Omega_6)}\frac{sinh\left(y\sqrt{\Omega_{10}\ s^{\alpha+\beta}}\right)}{sinh\left(\sqrt{\Omega_{10}\ s^{\alpha+\beta}}\right)} \tag{22}$$

where:

$$\Omega_1=\frac{\phi_1}{\phi_2},\ \Omega_2=\Omega_1*Re,\ \Omega_3=\beta\ \Gamma(\beta),\ \Omega_4=\frac{\Omega_1\Omega_2}{\Omega_3},\ \Omega_5=M\sin(\theta)+K_{eff},$$

$$\Omega_6=\frac{\Omega_5}{\phi_2},\ \Omega_7=\frac{\phi_3}{\phi_2},\ \Omega_8=\frac{\phi_4}{\phi_2},\ \Omega_9=\frac{\mathrm{Pe}}{\beta\ \Gamma(\beta)},\ \Omega_{10}=\frac{\Pi_1}{\beta\ \Gamma(\beta)},$$

Many researchers [40,41] have utilized different numerical schemes to discover the Laplace inverse of many governed equations solutions. As the solution obtained in Eq. (15) is more complicated, we have also utilized the numerical algorithms, namely Stehfest and Tzou's methods, with precise forms as follows.

$$W_1(y,t)=\frac{ln(2)}{t}\sum_{i=1}^{\infty}C_k\overline{W_1}\left(y,k\frac{ln(2)}{t}\right),$$

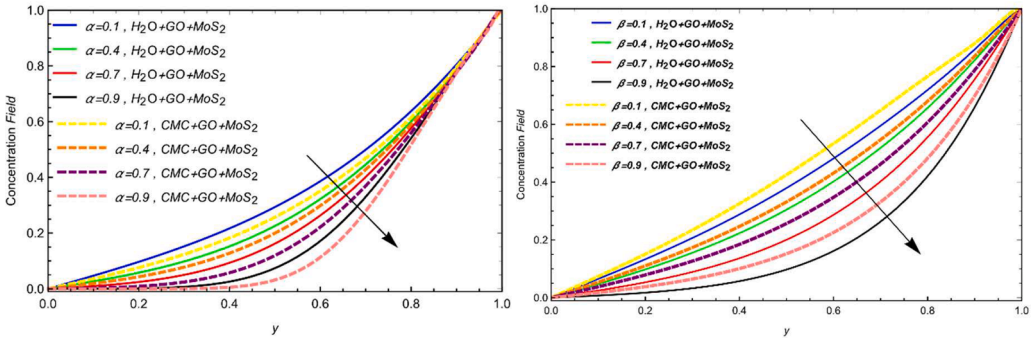

Fig. 3. Impact of fractional constraints α and β on concentration field with $t = 0.8$, φ = 0.02.

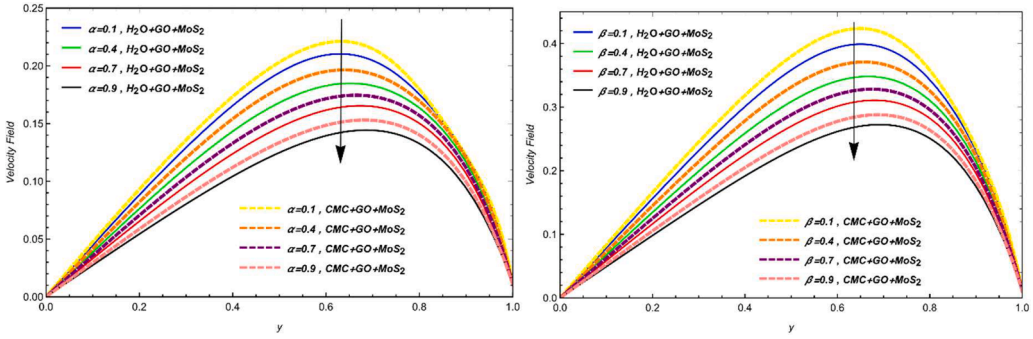

Fig. 4. Influence of fractional constraints α and β on $w_1(y,t)$ with $Pe = 3.5$, $Gr = 2.6$, $Gm = 4.5$, $Re = 2.0$, $M = 1.5$, $K = 0.9$, $\theta = \frac{\pi}{3}$, $t = 0.8$, $\varphi = 0.02$.

$$C_k = (-1)^{k+p} \sum_{j=\frac{k+1}{2}}^{min(k,p)} \frac{j^p (2j)!}{(p-j)!j!(i-1)!(k-1)!(2i-k)!},$$

$$W_1(y,t) = \frac{e^{4.7}}{t}\left[0.5\overline{W}_1\left(y,\frac{4.7}{t}\right) + Re\left\{\sum_{l=1}^{M}(-1)^l \overline{W}_1\left(y,\frac{4.7+l\pi i}{t}\right)\right\}\right],$$

Skin friction, Nusselt number, and Sherwood number

$$C_f = -\frac{\mu_{nf}}{\mu_f}\frac{\partial \overline{w}_1(y,s)}{\partial y}\bigg|_{y=0} = -\frac{\mu_{nf}}{\mu_f}\mathscr{L}^{-1}\left\{\frac{\partial w_1(0,t)}{\partial y}\right\}$$

$$Nu = -\frac{k_{nf}}{k_f}\frac{\partial \overline{T}_1(y,s)}{\partial y}\bigg|_{y=0} = -\frac{k_{nf}}{k_f}\mathscr{L}^{-1}\left\{\frac{\partial T_1(0,t)}{\partial y}\right\}$$

$$Sh = -D_{nf}\frac{\partial \overline{C}_1(y,s)}{\partial y}\bigg|_{y=0} = -D_{nf}\mathscr{L}^{-1}\left\{\frac{\partial C_1(0,t)}{\partial y}\right\}$$

5. Discussion of results

The current study investigates the analytical approaches to the conceptual fractional hybrid nanofluid simulation of flow over a porous material adjacent an infinitely perpendicular plate submerged in porous medium. This occurrence has been described in terms of partial PDEs, and these equations were subsequently translated into non-dimensional form using appropriate new non-dimensional components. To increase the viscosity of the hybrid nanofluid under investigation, we developed a fractional model based on the innovative Fractal fractional derivative operator description. This model includes a non-local and singular kernel that demonstrates the generalized memory ramifications. The Laplace integral transform technique solves the fractional formulation and generates correct solution formulations based on Mittag-Leffler functions for flow rate, concentration, and outside temperature.

The comparison of many hybrid nanofluids, including ($CMC + GO + MoS_2$) and ($H_2O + GO + MoS_2$), is shown in Figs. 2a & 2b. The effects of fractional parameters, such as (α, β) and Peclet number (Pe), on the temperature profile are also shown. These graphs show that increasing fractional parameter and Pe values are correlated with a decrease in the

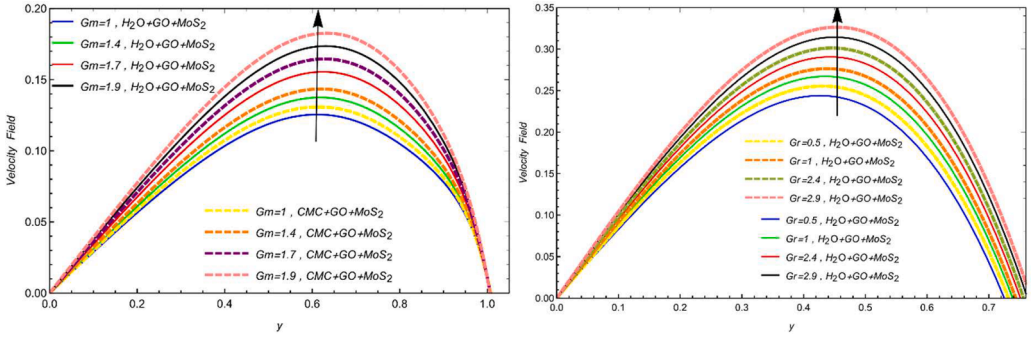

Fig. 5. Influence of mass grashof number Gm and heat grashof number Gr on $w_1(y,t)$ with $\alpha = \beta = 0.4$, $Pe = 3.5$, $Re = 2.0$, $M = 1.5$, $K = 0.9$, $\theta = \frac{\pi}{3}$, $t = 0.8$, $\varphi = 0.02$.

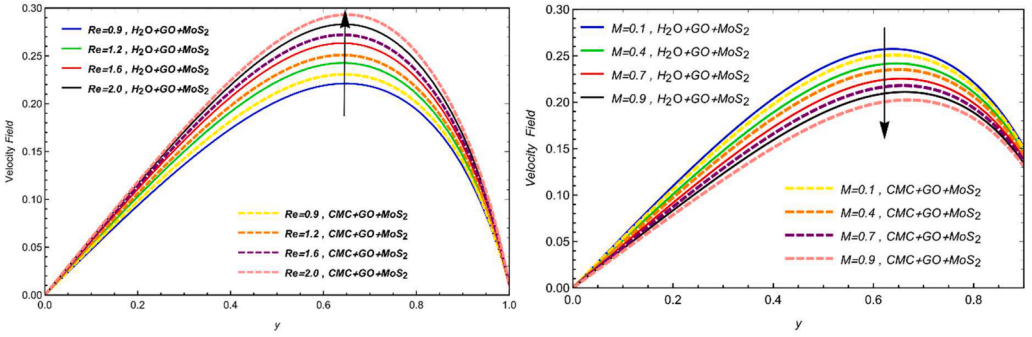

Fig. 6. Influence of Reynolds number Re and applied magnetic field M on $w_1(y,t)$ with $\alpha = \beta = 0.4$, $Pe = 3.5$, $Gr = 2.6$, $Gm = 4.5$, $K = 0.9$, $\theta = \frac{\pi}{3}$, $t = 0.8$, $\varphi = 0.02$.

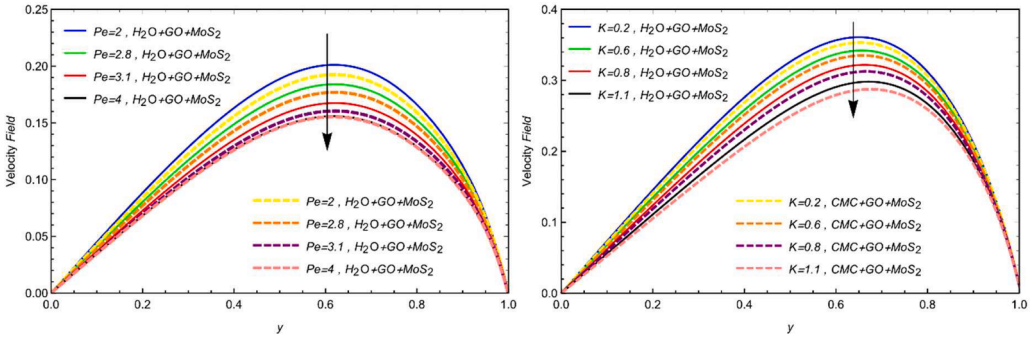

Fig. 7. Influence of Peclet number Pe and porosity parameter K on $w_1(y,t)$ with $\alpha = \beta = 0.4$, $Gr = 2.6$, $Gm = 4.5$, $Re = 2.0$, $M = 1.5$, $\theta = \frac{\pi}{3}$, $t = 0.8$, $\varphi = 0.02$.

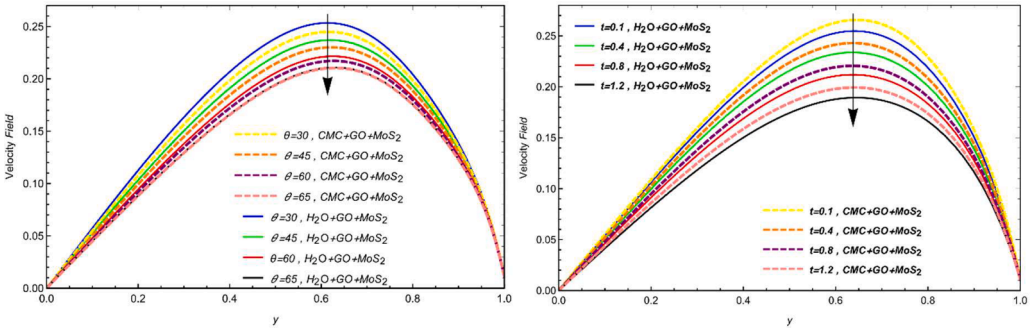

Fig. 8. Influence of inclination of magnetic field θ and time t on $w_1(y,t)$ with $\alpha = \beta = 0.4$, $Pe = 3.5$, $Gr = 2.6$, $Gm = 4.5$, $Re = 2.0$, $M = 1.5$, $K = 0.9$, $\varphi = 0.02$.

thermal profile. The Peclet number (Pe) is a dimensionless number employed in fluid science to assess the relevance of condensation vs absorption in a flow's direction. It means that molecules of fluid take a longer time to disperse compared to be directed by the flow. The flow is often greater diffusive than convection. Fluid particles travel gradually, and dispersion has a greater impact on flow than fluid's mass movement. As the (Pe) grows, the fluid's thermal distribution steepens at the limits. This indicates greater temperature shifts near the exterior walls or surfaces. As the (Pe) increases, the heating boundary layer thins. This causes a more dramatic thermal differential between most of the fluid and the outer layer. Higher (Pe) imply greater advection than diffusion, resulting in an improved mixture of fluids and equal temperature distribution in most flows. Furthermore, the thermal boundary layer may be controlled by the fractional parameters. Moreover, the assessment in the thermal profile generated by ($H_2O + GO + MoS_2$) is more progressive than ($CMC + GO + MoS_2$) in this case because of the unique physical features of specific nanoparticles.

Figs. 3a & 3b display the concentration profile for various fractional parameter α and β. Similar to the thermal field, the concentration field experiences a decrease when the fractional limitation increases. In fluid mechanics, fractional factors are generally related with calculus of fractions, a mathematical structure that stretches differentiation and integration to non-integer values. Using fractional characteristics improves monitoring and simulation of flow motion and content transfer in fluids. This allows for more realistic representations of complicated fluid phenomena. Fractional coefficients can affect the process of dispersion in a fluid. This determines how fast or gradually the concentration of chemicals distributes across the moving stream. In heat transfer applications, fractional quantities can impact thermo-diffusion operations. The concentration rate development caused by ($H_2O + GO + MoS_2$) is more advanced than ($CMC + GO + MoS_2$).

Representations of Figs.. 4a & 4b on velocity profile for different values of the fractional parameters(α, β). Fractional derivative products can be used in advection-diffusion algorithms to simulate movement in complicated surfaces, such as non-local effects. Fractional characteristics have a direct effect on the fluid's flow rate patterns. Changes in fractional variables considerably influence the fluid's movement pattern. In time-fractional simulations, the fractional value influences

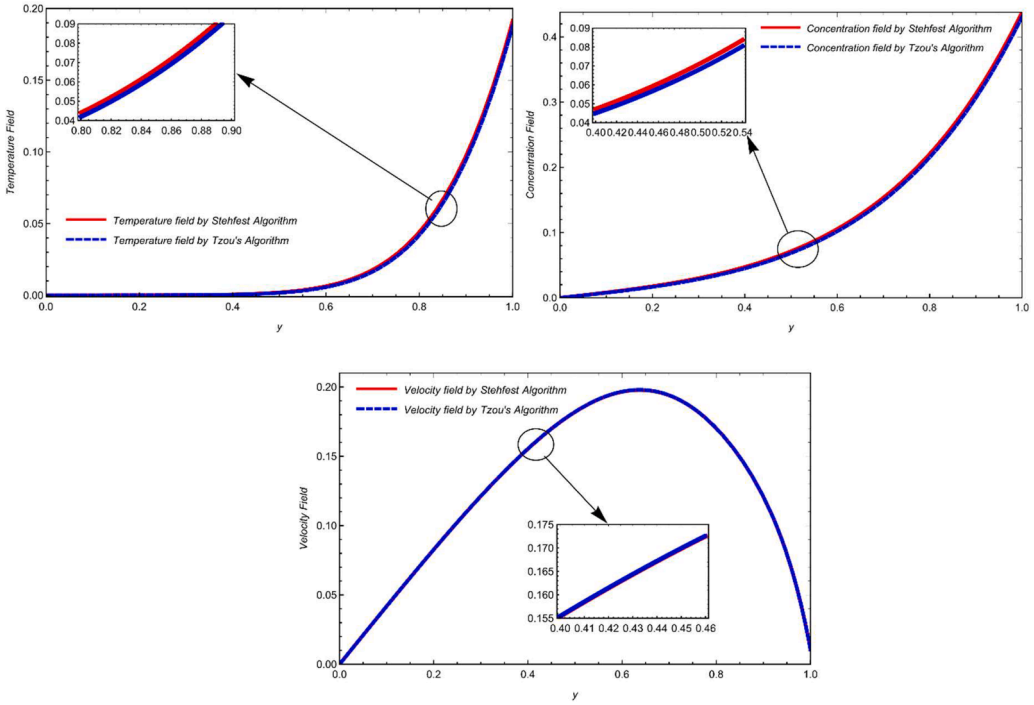

Fig. 9. Comparison of numerical schemes (Stehfest and Tzou's) on temperature, concentration, and velocity profiles.

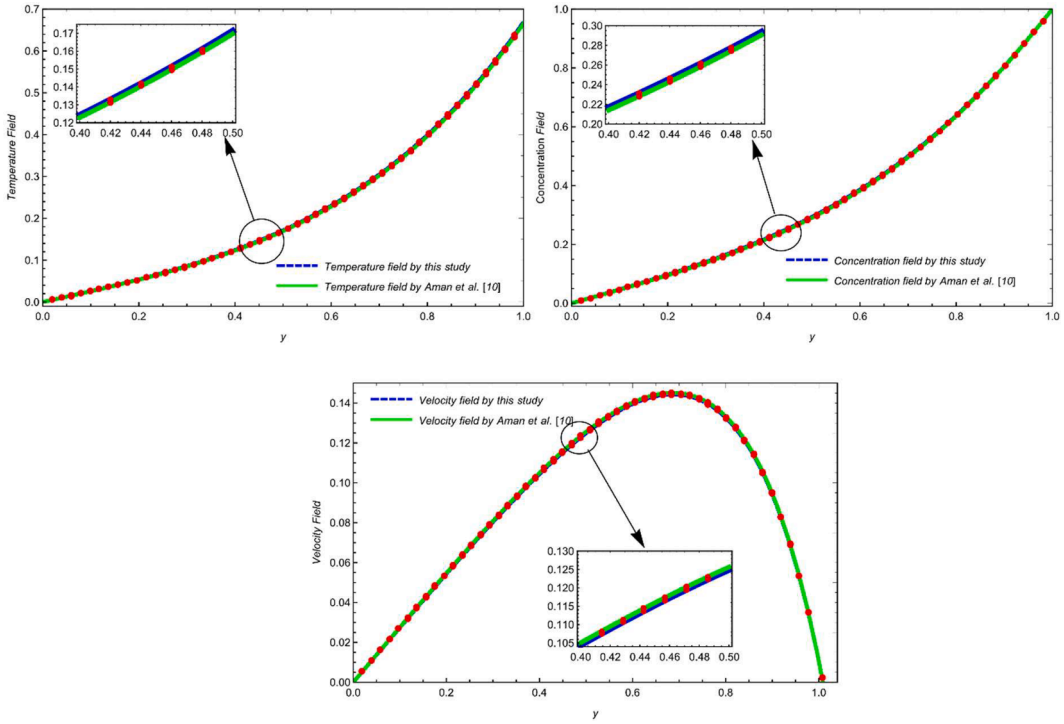

Fig. 10. Assessment of this study results with the outcomes of Aman et al. [10].

how rapidly the velocity varies with time. A larger fractional order reduces variations in velocity. As a result, when fractional limitations increase, fluid speed decreases. Furthermore, because of the unique physical properties of some nanoparticles, like thermal field and the concentration rate development caused by ($H_2O + GO + MoS_2$) is more advanced than ($CMC + GO + MoS_2$) due to the physical implications of nanoparticles and base fluids. Figs. 5a and 5b show the impact of mass and heat gradients, represented by the integers Gr and Gm, on the velocity field. Fluid velocity increases as a result of an increase in buoyant forces brought on by a rise in Gr. Physically, buoyant forces increase with increasing heat, mass fraction, and fluid velocity.

Figs. 6a & 6b signifying the variation in *Re* and *M* for different hybrid nanofluids. This can be seen that with the variation of both constraints velocity will decline for M while speed up for *Re*. The *Re* is a dimensionless number employed in hydrodynamics to forecast the flow dynamics in various flow scenarios. Flow is typically laminar, with

Table 3
The evaluation of governed outcomes at various time intervals$t = 0.5$ and 2.0.

y	$T_1(y,t)$ for $t =$ 0.5	$T_1(y,t)$ for $t =$ 2.0	$C_1(y,t)$ for $t =$ 0.5	$C_1(y,t)$ for $t =$ 2.0	$w_1(y,t)$ for $t =$ 0.5	$w_1(y,t)$ for $t =$ 2.0
0.1	0.3137	0.8025	0.3572	0.4255	0.1859	0.2389
0.2	0.2799	0.8414	0.3596	0.4391	0.3708	0.4718
0.3	0.2474	0.8715	0.3632	0.4529	0.5525	0.6922
0.4	0.2159	0.8939	0.3669	0.4673	0.7273	0.8924
0.5	0.1853	0.9099	0.3692	0.4828	0.8889	1.0638
0.6	0.1556	0.9205	0.3686	0.4990	1.0278	1.1939
0.7	0.1269	0.9270	0.3635	0.5154	1.1295	1.2694
0.8	0.0996	0.9306	0.3517	0.5312	1.1732	1.2759
0.9	0.0743	0.9327	0.3323	0.5470	1.1422	1.2018

Table 4
Numerical study of nusselt number*Nu*, Sherwood number*Sh*and Skin frictionC_f.

α	*Nu*	*Sh*	C_f
0.1	0.313762	0.776292	0.270217
0.2	0.27999	0.780544	0.270178
0.3	0.247433	0.784304	0.269187
0.4	0.215943	0.787665	0.2661
0.5	0.185351	0.791701	0.259964
0.6	0.15563	0.798514	0.249389
0.7	0.126943	0.809947	0.232761
0.8	0.0996876	0.825101	0.20837
0.9	0.0743859	0.839167	0.172142

uniform, ordered levels of fluid and little interaction. Velocity variations are minimal, and fluid velocity is typically consistent throughout the flow. So, at increasing values of *Re*, the velocity profile tends to increase. As M grows, the velocity drops. This is accurate physically for large values of M since M increases the Lorentz forces, which have the tendency to slow velocity. As the intensity of the electromagnetic field grows, so do the Lorentz forces, thereby slowing the speed of the fluid. This reduces the total flow rate and may result to the formation of boundaries with greater velocity differences near solid substrates. In highly conductive fluids, damping is stronger, resulting in a more consistent velocity profile over the flow region. Figs. 7a & 7b depicts how the momentum field is affected by (K) and (Pe). As can be seen velocity decreases as K and Pe values increase for both types of considered hybrid nanofluids. The drag forces lessen as (K) is raised, which causes the velocity to fall. As Pe values rise, the viscous forces will become more powerful than the thermal forces, resulting in a drop in fluid velocity.

Figs. 8a & 8b are accomplished for the influence of inclined magnetic field and time values. It is evident that as both parameters are increased, the velocity profile shows a declining trend. This feature of velocity can be explained physically by the fluid being stiffer with an increase in the angle of the nanoparticles, which lowers nanofluid rate. Speediness for the hybrid nanofluid decreases through intensifying standards of θ. Graphic trend of the velocity profile reveals that $(H_2O + GO + MoS_2)$ have a higher value as compared to $(CMC + GO + MoS_2)$ suspension. Physically, it is because $(H_2O + GO + MoS_2)$ demeanors considerable hotness then it is operative in spite of being fewer thick. $(CMC + GO + MoS_2)$ mixed interruption has complex rate between all solutions measured here.

Figs. 9(a, b, and c) compare the numerical methods of Tzou and Stehfest for each profile. The significant overlap of the profile curves demonstrates the reliability and accuracy of the present study. This concurrence between the two numerical approaches validates the robustness of the current investigation's results and methodology. Furthermore, in Figs. 10 (a, b & c) the assessment of this learning is examined with attained consequences of Aman et al. [10]. Again overlapping of both curves signifying this study validity. In [10], the authors utilized the old definition of fractional derivatives, namely the Caputo-fractional derivative, whereas, in this study, we have employed the recent definition of fractional derivatives, namely the Fractal fractional derivative. But in Fig 10, the overlapping of all curves validates this study. At the end, an examination of numerical comparison of all regulated solutions generated at different time values using the researched numerical approaches is presented in Table 3. Furthermore, the numerical analysis of the *Nu*, *Sh*, $C_f$is examined in Table 4. Tables also demonstrate that these approaches meet the necessary boundary and starting requirements.

6. Conclusion

The unrestricted convective flow of an unstable and incompressible movement assorted with $(H_2O + GO + MoS_2)$ and $(CMC + GO + MoS_2)$ hybrid nanofluids is explored flowing over two parallel dispensed plates by means of Water and CMC as the base fluid. The Fractal fractional derivative, the most recent description of a fractional derivative, creates a fractional prototypical by extending the Laplace transformation. The presence of various limits on computed temperature, concentration, and momentum outline norms is visually depicted. Here is an outline of some significant findings from this investigation:

- An increase in the value of *Pe* slows down both momentum and thermal profiles.
- By lowering the value of fractional constraints, the concentration field expands.
- This method might be used in more advanced physical science classes with intricate geometry.
- The study's conclusions can support with proper explanation of practical data and the challenging of numerous estimates for solutions when necessary.
- Outcomes of this research are reinforced by the geometric structure outcomes as well as the data obtainable in Aman et al. [10]. The curves' interaction provides more evidence for the conclusions.
- In the assessment of nanofluids, Water based $(H_2O + GO + MoS_2)$ interruption has a more substantial stimulus as associated to $(CMC + GO + MoS_2)$ nanofluids.

CRediT authorship contribution statement

Ahmed M. Abed: Writing – original draft, Data curation, Conceptualization. **Hamna Shabbir:** Writing – original draft, Methodology, Investigation, Formal analysis. **Niat Nigar:** Writing – original draft, Resources, Investigation. **Ali Hasan Ali:** Writing – review & editing, Visualization, Software, Project administration. **Ali Raza:** Writing – review & editing, Validation, Supervision.

Declaration of competing interest

The authors declare that they have no known competing financial interests or personal relationships that could have appeared to influence the work reported in this paper.

Data Availability

No data was used for the research described in the article.

Acknowledgement

This study is supported via funding from Prince Sattam bin Abdulaziz University project number (PSAU/2024/R/1445).

References

[1] A. Atangana, Fractal-fractional differentiation and integration: connecting fractal calculus and fractional calculus to predict complex system, Chaos, Soli. Fract 102 (2017) 396–406.
[2] M. Mahboobtosi, K. Hosseinzadeh, D. Ganji, Entropy generation analysis and hydrothermal optimization of ternary hybrid nanofluid flow suspended in polymer over curved stretching surface, Int. J. Thermofl 20 (2023) 100507.
[3] H.A. Prince, A. Ghosh, M.M.H. Siam, M.A.H. Mamun, AI predicts MHD double-diffusive mixed convection and entropy generation in hybrid-nanofluids for different magnetic field inclination angles by ANN, Int. J. Thermofl 19 (2023) 100383.
[4] V. Tangirala, R. Chen, J.F. Driscoll, Effect of heat release and swirl on the recirculation within swirl-stabilized flames, Combust. Sci. Technol 51 (1987) 75–95.
[5] R. Ahamed, M. Salehin, M.M. Ehsan, Thermal-hydraulic performance and flow phenomenon evaluation of a curved trapezoidal corrugated channel with E-shaped baffles implementing hybrid nanofluid, Heliyon. 10 (2024).
[6] M. Lax, D. Nelson, Maxwell equations in material form, Phy. Rev. B 13 (1976) 1777.
[7] J.A. Eastman, S. Choi, S. Li, W. Yu, L. Thompson, Anomalously increased effective thermal conductivities of ethylene glycol-based nanofluids containing copper nanoparticles, Appl. Phys. Lett. 78 (2001) 718–720.
[8] D.K. Devendiran, V.A. Amirtham, A review on preparation, characterization, properties and applications of nanofluids, Renew. Sustain. Ener. Rev 60 (2016) 21–40.
[9] M. Mahboobtosi, K. Hosseinzadeh, D. Ganji, Investigating the convective flow of ternary hybrid nanofluids and single nanofluids around a stretched cylinder: parameter analysis and performance enhancement, Int. J. Thermofl (2024) 100752.
[10] S. Aman, I. Khan, Z. Ismail, M.Z. Salleh, I. Tlili, A new Caputo time fractional model for heat transfer enhancement of water based graphene nanofluid: an application to solar energy, Results Phys. 9 (2018) 1352–1362.
[11] F. Khan, M.N. Karimi, O. Khan, A.K. Yadav, A. Alhodaib, A.E. Gürel, et al., A hybrid MCDM optimization for utilization of novel set of biosynthesized nanofluids on thermal performance for solar thermal collectors, Int. J. Thermofl 22 (2024) 100686.
[12] A. Raza, O.V. Stadoleanu, A.M. Abed, A.H. Ali, M. Sallah, Heat transfer model analysis of fractional Jeffery-type hybrid nanofluid dripping through a poured microchannel, Int. J. Thermofl 22 (2024) 100656.
[13] R. Saidur, K. Leong, H.A. Mohammed, A review on applications and challenges of nanofluids, Renew. Sustain. Ener. Rev 15 (2011) 1646–1668.
[14] T. Hayat, S. Nadeem, Heat transfer enhancement with Ag–CuO/water hybrid nanofluid, Results Phys. 7 (2017) 2317–2324.
[15] G. Domairry, A. Aziz, Approximate analysis of MHD squeeze flow between two parallel disks with suction or injection by homotopy perturbation method, Math. Probl. Eng. 2009 (2009).
[16] A. Farooq, M. Kahshan, S. Saleem, M. Rahimi-Gorji, F.S. Al-Mubaddel, Entropy production rate in ciliary induced flows through cylindrical tubules under the consequences of Hall effect, J. Taiwan Inst. Chem. Eng. 120 (2021) 207–217.
[17] M.I. Asjad, M.D. Ikram, A. Akgül, Analysis of MHD viscous fluid flow through porous medium with novel power law fractional differential operator, Phys. Scr. 95 (2020) 115209.
[18] C. Yue, M.M. Khater, R.A. Attia, D. Lu, The plethora of explicit solutions of the fractional KS equation through liquid–gas bubbles mix under the thermodynamic conditions via Atangana–Baleanu derivative operator, Adv. Differ. Equ 2020 (2020) 1–12.
[19] H. Sun, Y. Zhang, S. Wei, J. Zhu, W. Chen, A space fractional constitutive equation model for non-Newtonian fluid flow, Commun. Nonl. Sci. Numer. Simul 62 (2018) 409–417.
[20] A.A. Arafa, Z. Rashed, S.E. Ahmed, Radiative flow of non Newtonian nanofluids within inclined porous enclosures with time fractional derivative, Sci. Rep. 11 (2021) 5338.
[21] T. Tayebi, A.J. Chamkha, Entropy generation analysis due to MHD natural convection flow in a cavity occupied with hybrid nanofluid and equipped with a conducting hollow cylinder, J. Therm. Anal. Calorim. 139 (2020) 2165–2179.
[22] S. Manjunatha, V. Puneeth, R. Anandika, B. Gireesha, Analysis of multilayer convective flow of a hybrid nanofluid in porous medium sandwiched between the layers of nanofluid, Heat Transf 50 (2021) 8598–8616.
[23] J.-W. Lee, H.-B. CHO, T. Nakayama, T. Sekino, S.-I. Tanaka, K. Minato, et al., Dye-sensitized solar cells using purified squid ink nanoparticles coated on TiO2 nanotubes/nanoparticles, J. Ceram. Soc. Japan 121 (2013) 123–127.
[24] M. Bahiraei, M. Jamshidmofid, M. Goodarzi, Efficacy of a hybrid nanofluid in a new microchannel heat sink equipped with both secondary channels and ribs, J. Mol. Liq. 273 (2019) 88–98.
[25] C. Mendoza, A. Valle, M. Castellote, A. Bahamonde, M. Faraldos, TiO2 and TiO2–SiO2 coated cement: comparison of mechanic and photocatalytic properties, App. Catal. B: Environ 178 (2015) 155–164.
[26] A. Xu, D. Zhang, Y. Gan, Advances in the kinetics of heat and mass transfer in near-continuous complex flows, Front. Phys. 19 (2024) 42500.
[27] V. Kumar, P. Ram, K. Sharma, Entropy generation on inclined magnetize double diffusive convective transportation of radiative Casson nanofluid in porous medium with source/sink, Modern Phy. Lett. B (2024) 2450424.
[28] N. Yilmaz, A.S. Bakhtiyarov, R.N. Ibragimov, Experimental investigation of Newtonian and non-Newtonian fluid flows in porous media, Mech. Res. Commun. 36 (2009) 638–641.
[29] R. Agarwal, S.D. Purohit, Kritika, Introduction to fractional calculus and modelling. Modeling Calcium Signaling: A Fractional Perspective, Springer, 2024, pp. 1–28, ed.
[30] S. Abbas, M. Ahmad, M. Nazar, M. Amjad, H. Ali, A.Z. Jan, Heat and mass transfer through a vertical channel for the Brinkman fluid using Prabhakar fractional derivative, Appl. Therm. Eng. 232 (2023) 121065.
[31] K. Gangadhar, T. Sujana Sree, T. Thumma, Impact of Arrhenius energy and irregular heat absorption on generalized second grade fluid MHD flow over nonlinear elongating surface with thermal radiation and Cattaneo–Christov heat flux theory, Modern Phy. Lett. B 38 (2024) 2450077.
[32] Z. Shah, M.A.Z. Raja, W.A. Khan, M. Shoaib, V. Tirth, A. Algahtani, et al., Computational intelligence paradigm with Levenberg-Marquardt networks for dynamics of Reynolds nanofluid model for Casson fluid flow, Tribol. Int. 191 (2024) 109180.
[33] N. Almutairi, S. Saber, Application of a time-fractal fractional derivative with a power-law kernel to the Burke-Shaw system based on Newton's interpolation polynomials, MethodsX. 12 (2024) 102510.
[34] K.A. Abro, A. Atangana, Mathematical analysis of memristor through fractal-fractional differential operators: a numerical study, Math. Methods Appl. Sci. 43 (2020) 6378–6395.
[35] M. Arif, P. Kumam, W. Kumam, A. Akgul, T. Sutthibutpong, Analysis of newly developed fractal-fractional derivative with power law kernel for MHD couple stress fluid in channel embedded in a porous medium, Sci. Rep. 11 (2021) 20858.
[36] A. Akgül, J.A. Conejero, Fractal fractional derivative models for simulating chemical degradation in a bioreactor, Axioms 13 (2024) 151.
[37] S. Murtaza, E.A. Ismail, F.A. Awwad, E. Bonyah, A.M. Hassan, M.S. Khan, et al., Parametric simulations of fractal-fractional non-linear viscoelastic fluid model with finite difference scheme, AIP. Adv. 14 (2024).
[38] A. Raza, S.U. Khan, M.I. Khan, S. Farid, T. Muhammad, M.I. Khan, et al., Fractional order simulations for the thermal determination of graphene oxide (GO) and molybdenum disulphide (MoS2) nanoparticles with slip effects, Case Stud. Therm. Eng 28 (2021) 101453.
[39] K. Zheng, A. Raza, A.M. Abed, H. Khursheed, L.F. Seddek, A.H. Ali, et al., New fractional approach for the simulation of (Ag) and (TiO2) mixed hybrid nanofluid flowing through a channel: fractal fractional derivative, Case Stud. Therm. Eng 45 (2023) 102948.
[40] A.U. Awan, S. Riaz, K.A. Abro, A. Siddiqa, Q. Ali, The role of relaxation and retardation phenomenon of Oldroyd-B fluid flow through Stehfest's and Tzou's algorithms, Nonlin. Eng 11 (2022) 35–46.
[41] M. Imran, S. Sarwar, M. Abdullah, I. Khan, An analysis of the semi-analytic solutions of a viscous fluid with old and new definitions of fractional derivatives, Chinese J. Phy 56 (2018) 1853–1871.